HHS Public Access

Author manuscript

Biol Psychiatry. Author manuscript; available in PMC 2024 November 01.

Published in final edited form as:

Biol Psychiatry. 2023 November 01; 94(9): 706–720. doi:10.1016/j.biopsych.2023.02.008.

NMDAR-Arc signaling is required for Memory Updating and is disrupted in Alzheimer's Disease

Liuqing Yang[1], **Wenxue Liu**[1,4], **Linyuan Shi**[1], **Jing Wu**[1], **Wenchi Zhang**[1], **Yang-An Chuang**[1], **Javier Redding-Ochoa**[2], **Alfredo Kirkwood**[1], **Alena V. Savonenko**[2,*], **Paul F. Worley**[1,3,5,*]

[1]The Solomon H. Snyder Department of Neuroscience, Johns Hopkins University School of Medicine, Baltimore, MD 21205, USA.

[2]Department of Pathology, Johns Hopkins University School of Medicine, Baltimore, MD 21205, USA.

[3]Department of Neurology, Johns Hopkins University School of Medicine, Baltimore, MD 21205, USA.

[4]Current address: Department of Thoracic and Cardiovascular Surgery, Affiliated Drum Tower Hospital of Nanjing University Medical School, Institute of Cardiothoracic Vascular Disease, Nanjing University, Nanjing 210008, China

[5]Lead Contact

Abstract

Background: Memory deficits are central to many neuropsychiatric diseases. During acquisition of new information memories can become vulnerable to interference, yet mechanisms that underlie interference are unknown.

Methods: We describe a novel transduction pathway that links NMDAR to AKT signaling via the IEG Arc, and evaluate its role in memory. The signaling pathway is validated using biochemical tools and genetic animals, and function is evaluated in assays of synaptic plasticity and behavior. The translational relevance is evaluated in human postmortem brain.

*Correspondence: Alena V. Savonenko asavone1@jhmi.edu; Paul F. Worley pworley1@jhmi.edu.

Author contributions

L.Y., A.V.S. and P.F.W. designed the experiments. L.Y. performed most of the biochemical experiments. W.L. performed electrophysiology experiments. L.S. performed mouse behavioral experiments. J.W. investigated detailed Arc-p55PIK interaction and generated *p55PIK cKO* mouse. W.Z. identified Arc binding motifs in NMDA receptor. Y.C. generated rabbit polyclonal anti-p55PIK antibody and *Arc*^{F217F} knock-in mouse. J.R. prepared human AD and control brain samples. A.K. supervised electrophysiology experiments. A.V.S. supervised mouse behavioral experiments. L.Y., A.V.S. and P.F.W prepared the manuscript.

Declaration of interests

Disclaimer: This work was prepared while Dr. Alena Savonenko was employed at the Johns Hopkins University. The opinions expressed in this article are the author's own and do not reflect the view of the National Institutes of Health, the Department of Health and Human Services, or the United States government.

The authors report no biomedical financial interests or potential conflicts of interest.

Results: Arc is dynamically phosphorylated by CaMKII and binds the NMDA receptor (NMDAR) subunits NR2A/NR2B and a previously unstudied PI3K adaptor p55PIK (*PIK3R3*) *in vivo* in response to novelty or tetanic stimulation in acute slices. NMDAR-Arc-p55PIK recruits p110α PI3K and mTORC2 to activate AKT. NMDAR-Arc-p55PIK-PI3K-mTORC2-AKT assembly occurs within minutes of exploratory behavior and localizes to sparse synapses throughout hippocampus and cortical regions. Studies using conditional (Nestin-Cre) p55PIK deletion mice indicate that NMDAR-Arc-p55PIK-PI3K-mTORC2-AKT functions to inhibit GSK3 and mediates input-specific metaplasticity that protects potentiated synapses from subsequent depotentiation. *p55PIK cKO* mice perform normally in multiple behaviors including working-memory and longterm memory tasks but exhibit deficits indicative of increased vulnerability to interference in both short-term and long-term paradigms. The NMDAR-AKT transduction complex is reduced in postmortem brain of individuals with early Alzheimer's disease.

Conclusions: A novel function of Arc mediates synapse-specific NMDAR-AKT signaling and metaplasticity that contributes to memory updating and is disrupted in human cognitive disease.

Keywords

NMDA receptor; Arc; PI3K; metaplasticity; interference; Alzheimer's disease

Introduction

Current models of memory imagine ensembles of neurons that are competitively connected or disconnected by mechanisms of synaptic plasticity: principally long-term potentiation (LTP) and long-term depression (LTD) (1,2). The most common forms of LTP and LTD are dependent on NMDA receptor (NMDAR) activation and consequent influx of Ca^{2+} at synapses that activates CaMKII or calcineurin, respectively (3). NMDARs can also induce forms of plasticity that do not alter the strength of synapses, but rather, change the capacity of synapses for future plasticity. This is termed metaplasticity, and while models have been suggested the role of metaplasticity in memory remains hypothetical due to lack of understanding of molecular mechanisms that can provide selective manipulation (4). Here, we report that in response to NMDAR activity, the immediate early gene (IEG) Arc binds NMDAR subunits NR2A/NR2B and the phosphoinositide 3-kinase (PI3K) adaptor protein p55PIK to activate PI3K p110α, mTORC2, and AKT and thereby inhibit GSK3 to evoke metaplasticity that maintains the strength of recently potentiated synapses.

p55PIK (*PIK3R3*) is a previously unstudied member of the p85 class 1A PI3K adaptors (Figure 1B) (5,6). We developed a brain-specific conditional *PIK3R3* genetic deletion model (*p55PIK cKO*) and found that p55PIK is not required for brain development, neuronal growth factor signaling, or organismal viability. The selective role of p55PIK in transducing NMDAR-Arc-p55PIK-PI3K-mTORC2-AKT signaling provided an opportunity to examine the role of this pathway in synaptic physiology and behavior without altering canonical functions of NMDAR, Arc, or other components of the signaling pathway. Hippocampal slice recordings from *p55PIK cKO* mice demonstrated preservation of all conventional forms of NMDAR- and mGluR-dependent synaptic plasticity. Further analysis revealed a deficit in the metaplastic effect of NMDA-LTP to inhibit LTD. This suggested that LTP in *p55PIK cKO* mice *in vivo* should be as stable as that in wild type mice so

long as potentiated synapses do not later receive competing inputs. Consistent with this notion, *p55PIK cKO* mice exhibit normal performance in multiple behavioral and memory tests yet exhibit deficits in their ability to update either long-term spatial memories or short-term social recognition memories. A shared feature is that attempted acquisition of new information results in deterioration of performance in tasks that depend on previously acquired information. We interpret this deficit within the context of the associated synaptic physiology to indicate increased vulnerability to cognitive interference. Interestingly, human subjects demonstrate increased vulnerability to cognitive interference in association with mild cognitive impairment (7,8). We examined the translational relevance to human cognitive disease and report disruption of the NMDAR-Arc-AKT signaling complex in early-stage Alzheimer's disease (AD).

Methods and Materials

Transgenic mice generation

PIK3R3^{flox} and *Arc*^{P217F} knock-in mice were generated in Transgenic Core Laboratory at Johns Hopkins University (JHU) School of Medicine. *PIK3R3*^{flox} and *Arc*^{P217F} were validated by genomic PCR and Sanger sequencing. Conditional *p55PIK* brain-specific knockout was achieved by a two-step breeding scheme with *Nestin-Cre* mice. *PIK3R3*$^{flox/flox}$ mice were first bred with *Nestin-Cre* mice to generate *PIK3R3*$^{flox/flox}$;*Nestin-Cre* offspring. *PIK3R3*$^{flox/flox}$;*Nestin-Cre(heterozygote)* mice were further bred with *PIK3R3*$^{flox/flox}$ mice to produce *Control* (*PIK3R3*$^{flox/flox}$ without *Nestin-Cre*) and *p55PIK cKO* (with *Nestin-Cre*) littermates for electrophysiology and behavior experiments. *p55PIK cKO* was validated by genomic PCR and immunoblotting. All mice were housed under pathogen-free conditions at JHU Research Animal Facilities following the guidelines of JHU Animal Care and Use Committee.

Novel environment exploration

Mice were kept in a satellite facility close to the lab for at least two days before experiment. For basal group, mice were euthanized directly from home cage for brain dissection. For exploration groups, mice were put into a 60 cm (length) X 40 cm (width) X 20 cm (height) plastic box with toys of different colors and shapes (environmental enrichment, EE). Mice were euthanized for brain dissection at different time points during or after exploration. For brief exploration groups, mice were put into EE box for 5 min and then put back into their home cage for another 55 min, 1 hr, 2 hr, or 4 hr before sacrifice and brain dissection.

Brain lysate preparation and immunoprecipitation (IP)

Mouse forebrains or cortices were dissected in ice-cold PBS and stored in −80°C. Frozen tissues were later homogenized by sonication in RIPA buffer (PBS pH 7.4, 5 mM EDTA, 5 mM EGTA, 1% Triton X-100, 0.1% SDS, protease inhibitor cocktail and phosphatase inhibitor). Brain lysates were centrifuged at 16,000 g for 10 min for immunoblotting and 200,000 g for 30 min for IP to preclear incompletely solubilized components. Supernatants were diluted to a final concentration of 1 mg/ml total protein. IP was done using mouse monoclonal Arc antibody generated in this lab following standard procedures.

Proximity ligation assay

Mice were anesthetized with 50 mg/kg Pentobarbital from home cage or after 5 min EE exploration. Perfusion and brain fixation were done following standard procedures. Brain slices of 10 <m thickness were collected for Duolink® proximity ligation assay (Millipore Sigma Inc.) following manufacturer's instructions.

Electrophysiology

Hippocampal slices were prepared from 6-8 weeks old mice as described previously (9,10). Field excitatory postsynaptic potentials (fEPSPs) were recorded from the stratum radiatum of CA1 region using a 2-3 Ω borosilicate glass microelectrode filled with ACSF. Schaffer Collateral afferents was stimulated using concentric bipolar stimulating electrode (FHC Inc.) at 0.033 Hz with 0.2 ms pulses. NMDAR-LTP was induced using high-frequency stimulation consisted of four 100 Hz epochs. LTD and depotentiation were elicited using paired-pulses of 50 ms interstimulus interval (ISI) repeated at 1Hz (PP-1Hz) for 15 min.

Mouse behavior experiments

All experiments were done following the guidelines of the Johns Hopkins University Animal Care and Use Committee. *PIK3R3*$^{flox/flox}$ (*Control*) and *PIK3R3*$^{flox/flox}$; *Nestin-Cre* (*p55PIK cKO*) were 3-6 months old male littermates. All mice for behavioral tests were kept in reversed diurnal room at least one week before experiment. Behavioral performances in the Open Field, Y Maze, Radial Water Maze, and Fear Conditioning tests were recorded by a computer-based video tracking system (ANY-maze, Stoelting Co., IL). Detailed methods and materials are in supplemental information.

Results

Arc couples NMDAR to p55PIK-PI3K.

Previously, we demonstrated that Arc binds the NMDAR subunits NR2A and NR2B (11). We confirmed NMDAR-Arc binding *in vivo* using *Arc KO* (*Arc*$^{-/-}$) mice, and further confirmed that binding is mediated by the N-lobe GAG domain binding pocket using *Arc(P217F)* (*Arc*$^{P217F/P217F}$) mutant mice (Figure S1 A-F). Discovery of the NMDAR-Arc-PI3K signaling pathway emerged from studies of Arc that identified p55PIK as a candidate interactor [Figure 1A, see also (12)]. *p55PIK* mRNA is broadly expressed in neurons of the forebrain (6) (Figure S2A) and the gene product is similar to, but distinct from *PIK3R1* encoded p85α, p55α, or p50α (Figure 1B).

p55PIK is encoded by the gene *PIK3R3* and includes two SH2 domains and an interSH2 (iSH2) domain (Figure 1B). A crystal structure of the iSH2 domain of p85α identifies two helixes that are highly conserved in p55PIK (Figure S2B and S2C). Helix 1 of p85α interacts with p110α (13,14). p55PIK transgene expressed in HEK 293T cells co-immunoprecipitates (co-IPs) with Arc (Figure 1C). This interaction was also reconstituted using purified, bacterially-expressed proteins that revealed direct binding of Arc with the predicted iSH2 helix 2 of p55PIK (Figure 1D). In contrast to Arc-NR2A/2B binding that is mediated by Arc's GAG domain, Arc-p55PIK binding requires the N-terminal half of Arc (Figure 1E). The Arc-p55PIK interaction is specific to p55PIK since the iSH2 domain

of p85α does not interact with Arc (Figure 1F). The high degree of homology of helix 1 of *PIK3R1* and *PIK3R3* suggests that p55PIK interacts with p110α. Consistent with this prediction, Arc co-IPs p110α when co-expressed with p55PIK but not when co-expressed with p85α (Figure 1G).

We generated a brain-specific conditional deletion model of *PIK3R3* (*PIK3R3*$^{flox/flox}$; *Nestin-Cre,* subsequently termed *p55PIK cKO*) (Figures 1H, 1I and S2D). *p55PIK cKO* mice are viable and do not exhibit obvious changes in viability or growth compared to *Control* (*PIK3R3*$^{flox/flox}$). Primary neuronal cultures generated from *p55PIK cKO* cortex grew like neurons from *Control* cortex and exhibited insulin- and growth factor- (complete medium) induced increases of phosphorylated GSK3 (Figure S2E). We confirmed that p55PIK protein was absent in lysates from *p55PIK cKO* forebrain (Figure 1I) and found that p55PIK antibody co-IPed Arc from *Control* but not *p55PIK cKO* forebrain (Figure 1J). Moreover, NR2A co-IPed p110α from *WT* but not *Arc*$^{-/-}$ or *p55PIK cKO* forebrain lysate (Figure 1K). PI3K activity that co-IPs with p55PIK is reduced in *Arc*$^{-/-}$ brain lysate indicating that Arc enhances p55PIK-PI3K association (Figure 1L).

Arc and p55PIK mediate NMDAR-AKT activation in brain.

In canonical signaling PI3K phosphorylates phosphoinositides (PI) to generate PI(3,4,5)P that recruits PI3P-dependent kinase 1 (PDK1), which phosphorylates AKT(T308), and mTORC2, which phosphorylates AKT(S473) (15) (Figure 2A). Analysis of *p55PIK cKO* brain lysate revealed a reduction of AKT(pS473) but no change of AKT(pT308) (Figure 2B). Analysis of *Arc*$^{-/-}$ brain lysate revealed a similar selective reduction of AKT(pS473) but no change of AKT(pT308) (Figure 2B). Accordingly, we focused on mTORC2 activation. mTORC2 complex assembly is mediated by Sin1 recruitment to PI3P-containing membranes and co-assembly with Rictor and mTor (16-18) (Figure 2A). Sin1 pulldown of mTor, or Rictor pulldown of mTor, were similarly reduced in *Arc*$^{-/-}$ and *p55PIK cKO* brain lysates (Figure 2C and 2D) indicating a reduction of mTORC2 complex. Consistent with the requirement of AKT(pS473) for AKT activation, pGSKα(S21) and pGSK3ß(S9) were reduced in *Arc*$^{-/-}$ and *p55PIK cKO* brain lysates without changes of total GSK3ß (Figure 2E).

NMDAR activation increases phosphorylation of AKT(pS473) (19). Consistent with this observation, systemic administration of the non-competitive NMDAR antagonist MK-801 (1 mg/kg i.p. for 1 hr) reduced AKT(pS473) and GSK3ß(pS9) in *WT* mouse forebrain lysate (Figure 2F). By contrast, AKT(pS473) and GSK3ß(pS9) in *Arc*$^{-/-}$ and *p55PIK cKO* brain lysate were reduced compared to *WT* and were not changed after MK-801 administration, indicating that Arc and p55PIK are required to establish basal NMDAR-mediated AKT activity in brain.

NMDA-Arc-p55PIK assembly is enhanced by CaMKII phosphorylation of Arc.

MK801 administration (1 mg/kg i.p. for 1 hr) reduced the co-IP of NMDAR with Arc (Figure 3B). We reconstituted the NMDAR-Arc interaction in HEK 293T cells by co-expressing NR1 with either NR2A or NR2B and noted the Arc-NR2A and Arc-NR2B

interactions were enhanced by co-expression of CaMKIIα and inclusion of Ca^{2+} and calmodulin in lysis buffer (Figure 3C).

Consistent with prior studies, CaMKII co-IPed with NMDAR constructed with NR2B but not NR2A (20) suggesting that the enhanced association of Arc with NR1-NR2A does not require co-assembly of CaMKII. Co-expression of activated/calmodulin-independent CaMKII(T286D), but not kinase dead CaMKII(K42M), markedly increased Arc association with NR2A (Figure 3D). CaMKII phosphorylates Arc(S260) and is predicted to phosphorylate Arc(T278) (21), and we confirmed that Arc(pS260) increases in immunoprecipitates from cells expressing CaMKII(T286D) with NR1/NR2A (Figure 3E). Arc phosphomimic [Arc(S260D, T278D)] exhibited enhanced co-IP with NR1/NR2A compared to WT Arc with a corresponding increase of p55PIK (Figure 3F). Findings suggest CaMKII phosphorylation of Arc potentiates its binding to the NMDAR and assembly of the NMDAR-Arc-p55PIK complex.

NMDAR-Arc-p55PIK-AKT complex forms rapidly in an enriched environment.

To examine the hypothesis that behavioral activation might increase NMDAR-Arc complex formation and NMDAR-AKT signaling, we monitored NR2A co-IP with Arc after transferring mice from their home cage to an enriched environment (EE, Figure 4A-B). NR2A-Arc co-IP increased after 5 min and remained elevated after 60 min. The increase of NR2A-Arc co-IP at 5 min was not associated with an increase of total Arc protein, but Arc along with CaMKIIß and activated CaMKIIα&ß shifted from the Triton-soluble to Triton-resistant fraction that is enriched for NR2A (Figure S3A). Our Arc(p260) Ab was not sufficiently sensitive to directly detect Arc phosphorylation *in vivo*. Arc presence in the Triton resistant fraction remained elevated at 60 min while CaMKIIß and non-phosphorylated CaMKIIα&ß returned to the Triton soluble fraction (Figure S3A). Increased AKT(pS473) and GSK3ß(pS9) paralleled the time course of Arc-NMDAR co-IP (Figure S3B). Environmental enrichment did not increase AKT(pS473) or GSK3ß(pS9) in *p55PIK cKO* mice (Figure S3B). Mice that experienced 5 min of EE followed by 55 min in home cage showed sustained increased NR2A-Arc co-IP (Figure S3C), but this returned to baseline after an additional 2 hr in home cage (Figure S3D).

Dynamic NMDAR-Arc-p55PIK-AKT complex formation at sparse synapses *in vivo*.

We developed an assay to detect NR1 proximity to AKT (Figure 4C). Antibodies for NR1 and AKT were conjugated to short oligonucleotides that can be ligated and amplified with fluorescent nucleotides when within 40 nM (22). Consistent with biochemical assays, IHC of the NR1-AKT proximity signal was induced in mouse sensory cortex by 5 min of EE and was markedly diminished in $Arc^{-/-}$ and *p55PIK cKO* mice (Figure 4D-E). When imaged together with postsynaptic marker Homer the NR1-AKT proximity signal localized to a small percentage (~1% based on non-biased automated counts) of synaptic puncta in sensory cortex and molecular layer of the dentate gyrus (Figure 4F). NR1-AKT proximity signal was enriched throughout cortical areas including layers 2-3 of pre-frontal and sensory cortex, pyriform cortex, dorsal (but not ventral) blade of the molecular layer of the dentate gyrus and strata oriens and radiatum of CA1 and subiculum (Figure 4G-H). This sparsity and distribution is consistent with the biochemical model requiring the conjunction of behavior-

linked synaptic activity (23) and IEG expression (24), and the distributed neuronal encoding of behavior (25).

NMDAR-Arc-p55PIK-PI3K-mTORC2-AKT-GSK3 mediates the action of LTP to inhibit depotentiation.

Measures of baseline synaptic transmission of Schaffer-CA1 synapses in acute hippocampal slices were not different between *p55PIK cKO* and littermate *controls* (*PIK3R3*$^{flox/flox}$) (Figure 5A-C and Figure S4A-D). We then examined standard forms of NMDAR-dependent synaptic plasticity including NMDAR-LTD induced by 1Hz stimulation and NMDAR-LTP induced by brief tetanic stimulation (Figure S4E-F). Both forms of NMDAR-dependent synaptic plasticity were similarly induced in *p55PIK cKO* and *control* mice. We also examined group 1 metabotropic receptor plasticity including LTD (mGluR-LTD) and LTP (mGluR-LTP) (Figure S4G-H). Again, both forms of mGluR-dependent plasticity were similarly induced in *p55PIK cKO* and *control* mice. We next examined NMDAR-metaplasticity. NMDAR-LTP in *p55PIK cKO* showed greater depotentiation in response to subsequent 1 Hz paired-pulse stimulation (Figure 5D). Depotentiation was specific to the stimulus input since it did not alter LTP induced by an independent input to the same population of neurons (Figure 5E). NMDAR-LTP in *Arc*$^{-/-}$ also showed greater depotentiation to subsequent 1 Hz paired-pulse stimulation (Figure 5F). We examined the dependence on *de novo* protein synthesis by incubating hippocampal slices with cycloheximide (120 μM) (Figure 5G) or anisomycin (10 μM) (Figure S4I) 30 min before recording and found both abolished the ability of NMDAR-LTP to prevent depotentiation. In slices pretreated with the GSK3 inhibitor SB415286 (10 μM), depotentiation following NMDAR-LTP was not different in *p55PIK cKO* compared to control slices (Figure 5H) consistent with a role for GSK3 inhibition in depotentiation (26). NMDAR-LTP stimulation also induced an significant increase of NR2A co-IP with Arc in hippocampal slices (Figure 5I), and while AKT(pS473) and GSK3ß(pS9) increased in response to tetanic stimulation in *control*, there was no increase of these molecular signatures of AKT activation in *p55PIK KO* (Figure S6J) indicating that p55PIK is required for coupling between LTP-AKT-GSK3, in contrast to a prior hypothetical model [1].

p55PIK is required for memory updating

We examined 3-6 months old male *p55PIK cKO* and littermate *control* mice in a series of standard behavior and memory tasks. Studies revealed no differences between genotypes in general behavioral traits such as anxiety levels, sensorimotor abilities (visual discrimination, swim speed, sensitivity to shock, startle response) or sensory-motor gating (prepulse inhibition) (Figure S5A-D). In a fear conditioning paradigm, *p55PIK cKO* mice exhibited long-term contextual and cued memory that was not different than *control* mice (Figure S5E-G). In the radial water maze reference memory task where animals learn to find the position of a hidden platform over two consecutive training days, there was no difference between genotypes in the number of errors or latency to find the platform (Figure 6A-B, S5H) and no difference in error rate when tested 20 hr later (long-term reference memory) (Figure 6C). Similarly, there were no differences in working memory as indicated by repeated visits to wrong arms in either the first trial (orientation trial) or during subsequent acquisition trials

(Figure 6D). Working memory tested in a classical Y maze was also not different (Figure S5C).

Further behavioral studies examined the notion that p55PIK might be required when there is competition between new and prior knowledge (27,28). We extended the radial maze task to include learning new positions of the submerged platform. The two-day radial water maze paradigm described above was continued for an additional 3 days, and the platform position was changed daily on days 3-5 (Figure 6A, E-G). During daily sessions on days 3-5, both genotypes showed the expected initial errors followed by improvement finding the new platform location. In contrast to *controls*, performance of *p55PIK cKO* mice deteriorated by the last trial indicating that new memories were not stable and were affected by between-trial interference (Figure 6E, Figure S5I). Analyses of errors after a 20 hr delay (during a next day's Orientation trial) revealed that *p55PIK cKO* mice visited a previous day's platform location significantly less than the *control* group (Figure 6F, Figure S5J). On days 4-5, *p55PIK cKO* mice made more errors before the 1st visit to the platform location from days 1-2 (reference memory) (Figure 6G, left) or the platform location of prior days 3 or 4 (Figure 6G, right). Considering that initial encoding and consolidation of the reference memory was not affected (Figure 6B and C), the cognitive deficit of the *p55PIK cKO* mice was not due to inability to create long-term memory traces, but rather an impairment in the ability to update the memory. This memory deficit impacted both new memories and the original reference memory, indicating interference between newly acquired and previously established memory traces.

Behavior suggestive of increased vulnerability to interference in *p55PIK cKO* was also observed in a brief memory paradigm based on social motivation (Figure 6H). *p55PIK cKO* and *control* mice showed identical motivation for social interaction (Figure 6I) but when tested for discrimination of the familiar and novel mouse, *p55PIK cKO* mice showed no discrimination (Figure 6J). Thus, as in the radial maze task, findings support the notion that assimilation of new information interferes with the original representation in *p55PIK cKO* mice.

NMDAR-AKT proximity complex is reduced in brain of individuals with Alzheimer's disease.

Human subjects diagnosed with MCI exhibit increased vulnerability to interference in short-term memory tasks (7,8). To examine the possibility that failure of NMDAR-AKT complex formation might contribute to cognitive deficits in AD, we developed a proximity ligation assay using NR2A and AKT antibodies (Figure 7A) and examined fresh frozen neocortex from two independent cohorts of individuals with pathologically confirmed AD versus age-matched controls. Cohort 1 primarily included individuals of late-stage AD with CERAD [Consortium to Establish a Registry for Alzheimer's Disease (29)] Score C and BRAAK [neurofibrillary pathology (30)] Score 4-6 while cohort 2 included primarily individuals of early-stage AD with CERAD Score B and BRAAK Score 2-3. The NR2A-AKT proximity signal was reduced in both AD cohorts relative to age-matched controls (Figure 7C and D). Immunoblots of the same samples revealed similar levels of NR2A, Arc, and AKT in control and AD samples indicating that reduced NR2A-AKT is not a consequence of a prominent

reduction of one of the constituents (Figure 7C and D). Total levels of CaMKIIα were also not different. However, phosphorylated CaMKII, indicative of CaMKII activity, was reduced in both AD cohorts relative to controls. In cohort 2, NMDAR-Arc co-IP and AKT(pS473) were also reduced in AD samples (Figure 7D), consistent with the role of NMDAR-Arc complex formation in activating AKT.

Discussion

Arc couples the NMDAR to synaptic PI3K-AKT-GSK3 signaling

The present study defines a multicomponent NMDAR-Arc-p55PIK-PI3K-mTORC2-AKT-GSK3 transduction pathway that underlies synapse-specific metaplasticity and implicates this pathway in memory updating. NMDAR-Arc binding is dependent on the Arc GAG domain N-lobe binding pocket consistent with prior structural studies (11). The same Arc binding pocket mediates interaction with TARP-AMPAR in the process of mGluR-LTD and homeostatic scaling. However, Arc's function in synaptic weakening is scaled by CaMKII phosphorylation since phosphorylation prevents Arc's oligomerization required to weaken synapses (21). Thus, local CaMKII activity defines the functional impact of Arc. These insights can be incorporated into synaptic tagging and cellular consolidation models of memory (31). At specific LTP-activated synapses Arc "tags" NMDARs and recruits AKT to prevent depotentiation, while at adjacent synapses within dendritic segments or inactive synapses cell-wide (with low CaMKII activity) Arc "inversely tags" TARP-AMPAR to scale-down synaptic strength (21,32) (Figure S5K).

Arc mRNA is rapidly transcribed and trafficked to dendrites (33), but these processes are not sufficiently rapid to provide a *de novo* source of Arc protein that is incorporated into the NMDAR-Arc-p55PIK-PI3K-mTORC2-AKT complex within 5 minutes. However, *de novo* Arc protein can be generated by reversal of stalled ribosomes in dendrites within 10 seconds (34). One caveat of our model is that we cannot directly detect phosphorylated Arc *in vivo* in response to EE possibly due to the limited sensitivity of our current phosphospecific Arc antibody and/or the sparsity of the NMDAR-Arc-AKT complex in brain. Nevertheless, CaMKII activity increases NR2A-Arc binding and phosphorylates Arc in reconstituted heterologous cells and Arc phosphomutants show enhanced co-assembly with NMDAR and p55PIK (Figure 3E-F).

Like Arc, the IEG Homer1a can stabilize NMDA-LTP by preventing depotentiation (35) and can also mediate homeostatic scaling down of excitatory synapses . Arc and Homer1a are transcriptionally induced following NMDAR activation and are co-expressed in the same pyramidal neurons (36). However, Homer1a expression peaks after Arc and Homer1a-dependent block of depotentiation requires concomitant dopamine D1 receptor mediated phosphorylation of mGluR5 and the prolyl isomerase Pin1 (35). The similarity of action and sequential expression suggest that NMDAR-Arc-p55PIK-PI3K-mTORC2-AKT and D1R-mGluR-Homer1a-Pin1-NMDAR represent sequential processes that initiate (NMDAR-Arc) and conditionally sustain (Homer1a-Pin1-NMDAR) behaviorally relevant ensembles of synaptically connected neurons (37).

Memory Updating and Interference

p55PIK cKO selectively impairs the ability to integrate new information with prior knowledge. Evidence of interference between previously learned and new information was observed in longterm spatial and short-term social tasks implicating the NMDAR-Arc-p55PIK-AKT pathway across different temporal, sensory, and motivation domains. In cognitive psychology the role of interference in memory updating is described in two settings (38). Learning can be disrupted shortly after an experience by task-related or unrelated behavior. Alternatively, long-term consolidated memory can be altered when it is retrieved in a specific context and reconsolidated with interfering information (27,39,40). These instances of altered memory parallel phenotypes in *p55PIK cKO* mice suggesting a role for NMDAR-Arc-p55PIK-AKT in mitigating the effects of interference. In the case of short-term memory, neurons that express Arc and create the NMDAR-AKT signaling complex may be preferentially incorporated into new ensembles generated in response to initial information. Neurons may require synaptic NMDAR-Arc-p55PIK-AKT established during the initial moments of the experience to distinguish initial from later information. Similarly, in long-term memory, synapses in which NMDAR-Arc-p55PIK-AKT signaling is activated during memory formation could be reactivated during retrieval based on the synaptic connectivity that defines the engram and would be protected against depotentiation during reconsolidation. If novelty is detected after retrieval, another wave of Arc expression could initiate NMDAR-Arc-p55PIK-AKT signaling in a different subset of synapses and neurons that may be connected to the first engram depending on the extent of overlap and be resistant to synaptic strength modulation during the next retrieval. This mechanism can support effective storage of new experiences without deterioration of previous experiences. It will be important to test the hypothesized role of NMDAR-Arc-p55PIK-AKT in preventing effects of interference in discrete circuits that mediate specific behaviors.

The challenge of memory updating can be appreciated from efforts in Artificial Intelligence (AI) to achieve “continual learning” or “progressive learning” (41). Current strategies incorporate aspects of natural intelligence including replay (42). However, performance typically declines as AI systems train on a second data set and can fail catastrophically (41). The challenge of memory updating is also revealed in human subjects with amnestic mild cognitive impairment (aMCI) who exhibit heightened vulnerability to interference (8). Interestingly, the memory-disruptive effect of interference is greatest immediately after training (7) consistent with failure of a rapid, task-related change of synaptic function. Interference based on competition between hippocampal circuits can prevent memory retrieval and has been implicated in memory failure in an Alzheimer’s amyloidosis model (43). The observation that NMDAR-AKT is reduced in AD brain (Figure 7) supports the notion that failure of the NMDAR-Arc-PI3K-AKT mechanism could contribute to vulnerability to interference and memory failure.

Supplementary Material

Refer to Web version on PubMed Central for supplementary material.

Acknowledgements

We thank Dr. Richard L. Huganir for NMDA receptor and CaMKII plasmids, Dr. Seung-Eon Roh for help with image analysis, Dr. Joshua Vogelstein for discussions of AI, Drs. David Linden and Lynn Nadel for reading the manuscript. This study was supported by MH053608, NS097966, AG065169, NARSAD Young Investigator Grant (27824) from the Brain & Behavior Research Foundation, and ADRC P30AG066507.

References

1. Dringenberg HC. The history of LONG-TERM potentiation as a memory mechanism: Controversies, confirmation, and some lessons to remember. Hippocampus. 2020 Sep;30(9):987–1012. [PubMed: 32442358]
2. Josselyn SA, Tonegawa S. Memory engrams: Recalling the past and imagining the future. Science. 2020 Jan 3;367(6473):eaaw4325. [PubMed: 31896692]
3. Lisman J. Glutamatergic synapses are structurally and biochemically complex because of multiple plasticity processes: long-term potentiation, long-term depression, short-term potentiation and scaling. Phil Trans R Soc B. 2017 Mar 5;372(1715):20160260. [PubMed: 28093558]
4. Abraham WC. Metaplasticity: tuning synapses and networks for plasticity. Nat Rev Neurosci. 2008 May;9(5):387–387. [PubMed: 18401345]
5. Gross C, Bassell GJ. Neuron-specific regulation of class I PI3K catalytic subunits and their dysfunction in brain disorders. Front Mol Neurosci [Internet]. 2014 [cited 2022 Aug 29];7. Available from: http://journal.frontiersin.org/article/10.3389/fnmol.2014.00012/abstract
6. Pons S, Asano T, Glasheen E, Miralpeix M, Zhang Y, Fisher TL, et al. The structure and function of p55PIK reveal a new regulatory subunit for phosphatidylinositol 3-kinase. Molecular and Cellular Biology. 1995 Aug;15(8):4453–65. [PubMed: 7542745]
7. Dewar M, Garcia YF, Cowan N, Della Sala S. Delaying interference enhances memory consolidation in amnesic patients. Neuropsychology. 2009 Sep;23(5):627–34. [PubMed: 19702416]
8. Dewar M, Pesallaccia M, Cowan N, Provinciali L, Della Sala S. Insights into spared memory capacity in amnestic MCI and Alzheimer's Disease via minimal interference. Brain and Cognition. 2012 Apr;78(3):189–99. [PubMed: 22261228]
9. Huang CC, Liang YC, Hsu KS. Characterization of the Mechanism Underlying the Reversal of Long Term Potentiation by Low Frequency Stimulation at Hippocampal CA1 Synapses. Journal of Biological Chemistry. 2001 Dec;276(51):48108–17. [PubMed: 11679581]
10. Wang H, Ardiles AO, Yang S, Tran T, Posada-Duque R, Valdivia G, et al. Metabotropic Glutamate Receptors Induce a Form of LTP Controlled by Translation and Arc Signaling in the Hippocampus. J Neurosci. 2016 Feb 3;36(5):1723–9. [PubMed: 26843652]
11. Zhang W, Wu J, Ward MD, Yang S, Chuang YA, Xiao M, et al. Structural Basis of Arc Binding to Synaptic Proteins: Implications for Cognitive Disease. Neuron. 2015 Apr;86(2):490–500. [PubMed: 25864631]
12. Chowdhury S, Shepherd JD, Okuno H, Lyford G, Petralia RS, Plath N, et al. Arc/Arg3.1 Interacts with the Endocytic Machinery to Regulate AMPA Receptor Trafficking. Neuron. 2006 Nov;52(3):445–59. [PubMed: 17088211]
13. Huang CH, Mandelker D, Schmidt-Kittler O, Samuels Y, Velculescu VE, Kinzler KW, et al. The Structure of a Human p110α/p85α Complex Elucidates the Effects of Oncogenic PI3Kα Mutations. Science. 2007 Dec 14;318(5857):1744–8. [PubMed: 18079394]
14. Miled N, Yan Y, Hon WC, Perisic O, Zvelebil M, Inbar Y, et al. Mechanism of Two Classes of Cancer Mutations in the Phosphoinositide 3-Kinase Catalytic Subunit. Science. 2007 Jul 13;317(5835):239–42. [PubMed: 17626883]
15. Fruman DA, Chiu H, Hopkins BD, Bagrodia S, Cantley LC, Abraham RT. The PI3K Pathway in Human Disease. Cell. 2017 Aug;170(4):605–35. [PubMed: 28802037]
16. Frias MA, Thoreen CC, Jaffe JD, Schroder W, Sculley T, Carr SA, et al. mSin1 Is Necessary for Akt/PKB Phosphorylation, and Its Isoforms Define Three Distinct mTORC2s. Current Biology. 2006 Sep;16(18):1865–70. [PubMed: 16919458]

17. Jacinto E, Facchinetti V, Liu D, Soto N, Wei S, Jung SY, et al. SIN1/MIP1 Maintains rictor-mTOR Complex Integrity and Regulates Akt Phosphorylation and Substrate Specificity. Cell. 2006 Oct;127(1):125–37. [PubMed: 16962653]

18. Liu P, Gan W, Chin YR, Ogura K, Guo J, Zhang J, et al. PtdIns(3,4,5) P_3-Dependent Activation of the mTORC2 Kinase Complex. Cancer Discov. 2015 Nov;5(11):1194–209. [PubMed: 26293922]

19. Sutton G, Chandler LJ. Activity-dependent NMDA receptor-mediated activation of protein kinase B/Akt in cortical neuronal cultures. J Neurochem. 2002 Sep;82(5):1097–105. [PubMed: 12358757]

20. Chen Q, He S, Hu XL, Yu J, Zhou Y, Zheng J, et al. Differential Roles of NR2A- and NR2B-Containing NMDA Receptors in Activity-Dependent Brain-Derived Neurotrophic Factor Gene Regulation and Limbic Epileptogenesis. Journal of Neuroscience. 2007 Jan 17;27(3):542–52. [PubMed: 17234586]

21. Zhang W, Chuang YA, Na Y, Ye Z, Yang L, Lin R, et al. Arc Oligomerization Is Regulated by CaMKII Phosphorylation of the GAG Domain: An Essential Mechanism for Plasticity and Memory Formation. Molecular Cell. 2019 Jul;75(1):13–25.e5. [PubMed: 31151856]

22. Alam MS. Proximity Ligation Assay (PLA). Current Protocols in Immunology. 2018 Nov;123(1):e58. [PubMed: 30238640]

23. Lu R, Liang Y, Meng G, Zhou P, Svoboda K, Paninski L, et al. Rapid mesoscale volumetric imaging of neural activity with synaptic resolution. Nat Methods. 2020 Mar;17(3):291–4. [PubMed: 32123393]

24. Guzowski JF, McNaughton BL, Barnes CA, Worley PF. Environment-specific expression of the immediate-early gene Arc in hippocampal neuronal ensembles. Nat Neurosci. 1999 Dec;2(12):1120–4. [PubMed: 10570490]

25. Kauvar IV, Machado TA, Yuen E, Kochalka J, Choi M, Allen WE, et al. Cortical Observation by Synchronous Multifocal Optical Sampling Reveals Widespread Population Encoding of Actions. Neuron. 2020 Jul 22;107(2):351–367.e19. [PubMed: 32433908]

26. Peineau S, Taghibiglou C, Bradley C, Wong TP, Liu L, Lu J, et al. LTP inhibits LTD in the hippocampus via regulation of GSK3beta. Neuron. 2007 Mar 1;53(5):703–17. [PubMed: 17329210]

27. Alonso A, van der Meij J, Tse D, Genzel L. Naïve to expert: Considering the role of previous knowledge in memory. Brain and Neuroscience Advances. 2020 Jan;4:239821282094868.

28. Fernández G, Morris RGM. Memory, Novelty and Prior Knowledge. Trends in Neurosciences. 2018 Oct;41(10):654–9. [PubMed: 30274601]

29. Fillenbaum GG, van Belle G, Morris JC, Mohs RC, Mirra SS, Davis PC, et al. Consortium to Establish a Registry for Alzheimer's Disease (CERAD): the first twenty years. Alzheimers Dement. 2008 Mar;4(2):96–109. [PubMed: 18631955]

30. Braak H, Alafuzoff I, Arzberger T, Kretzschmar H, Del Tredici K. Staging of Alzheimer disease-associated neurofibrillary pathology using paraffin sections and immunocytochemistry. Acta Neuropathol. 2006 Oct;112(4):389–404. [PubMed: 16906426]

31. Redondo RL, Morris RGM. Making memories last: the synaptic tagging and capture hypothesis. Nat Rev Neurosci. 2011 Jan;12(1):17–30. [PubMed: 21170072]

32. Okuno H, Akashi K, Ishii Y, Yagishita-Kyo N, Suzuki K, Nonaka M, et al. Inverse Synaptic Tagging of Inactive Synapses via Dynamic Interaction of Arc/Arg3.1 with CaMKIIβ. Cell. 2012 May;149(4):886–98. [PubMed: 22579289]

33. Steward O, Wallace CS, Lyford GL, Worley PF. Synaptic activation causes the mRNA for the IEG Arc to localize selectively near activated postsynaptic sites on dendrites. Neuron. 1998 Oct;21(4):741–51. [PubMed: 9808461]

34. Na Y, Park S, Lee C, Kim DK, Park JM, Sockanathan S, et al. Real-Time Imaging Reveals Properties of Glutamate-Induced Arc/Arg 3.1 Translation in Neuronal Dendrites. Neuron. 2016 Aug;91(3):561–73. [PubMed: 27397520]

35. Park JM, Hu JH, Milshteyn A, Zhang PW, Moore CG, Park S, et al. A prolyl-isomerase mediates dopamine-dependent plasticity and cocaine motor sensitization. Cell. 2013 Aug 1;154(3):637–50. [PubMed: 23911326]

36. Vazdarjanova A, McNaughton BL, Barnes CA, Worley PF, Guzowski JF. Experience-dependent coincident expression of the effector immediate-early genes arc and Homer 1a in hippocampal and neocortical neuronal networks. J Neurosci. 2002 Dec 1;22(23):10067–71. [PubMed: 12451105]

37. Marton TM, Hussain Shuler MG, Worley PF. Homer 1a and mGluR5 phosphorylation in reward-sensitive metaplasticity: A hypothesis of neuronal selection and bidirectional synaptic plasticity. Brain Res. 2015 Dec 2;1628(Pt A):17–28. [PubMed: 26187757]

38. Hardt O, Nader K, Nadel L. Decay happens: the role of active forgetting in memory. Trends in Cognitive Sciences. 2013 Mar;17(3):111–20. [PubMed: 23369831]

39. Schiller D, Monfils MH, Raio CM, Johnson DC, Ledoux JE, Phelps EA. Preventing the return of fear in humans using reconsolidation update mechanisms. Nature. 2010 Jan 7;463(7277):49–53. [PubMed: 20010606]

40. Wang SH, Morris RGM. Hippocampal-neocortical interactions in memory formation, consolidation, and reconsolidation. Annu Rev Psychol. 2010;61:49–79, C1–4. [PubMed: 19575620]

41. Flesch T, Balaguer J, Dekker R, Nili H, Summerfield C. Comparing continual task learning in minds and machines. Proc Natl Acad Sci USA [Internet]. 2018 Oct 30 [cited 2023 Jan 30];115(44). Available from: https://pnas.org/doi/full/10.1073/pnas.1800755115

42. Fayek HM, Cavedon L, Wu HR. Progressive learning: A deep learning framework for continual learning. Neural Netw. 2020 Aug;128:345–57. [PubMed: 32470799]

43. Poll S, Mittag M, Musacchio F, Justus LC, Giovannetti EA, Steffen J, et al. Memory trace interference impairs recall in a mouse model of Alzheimer's disease. Nat Neurosci. 2020 Aug;23(8):952–8. [PubMed: 32514139]

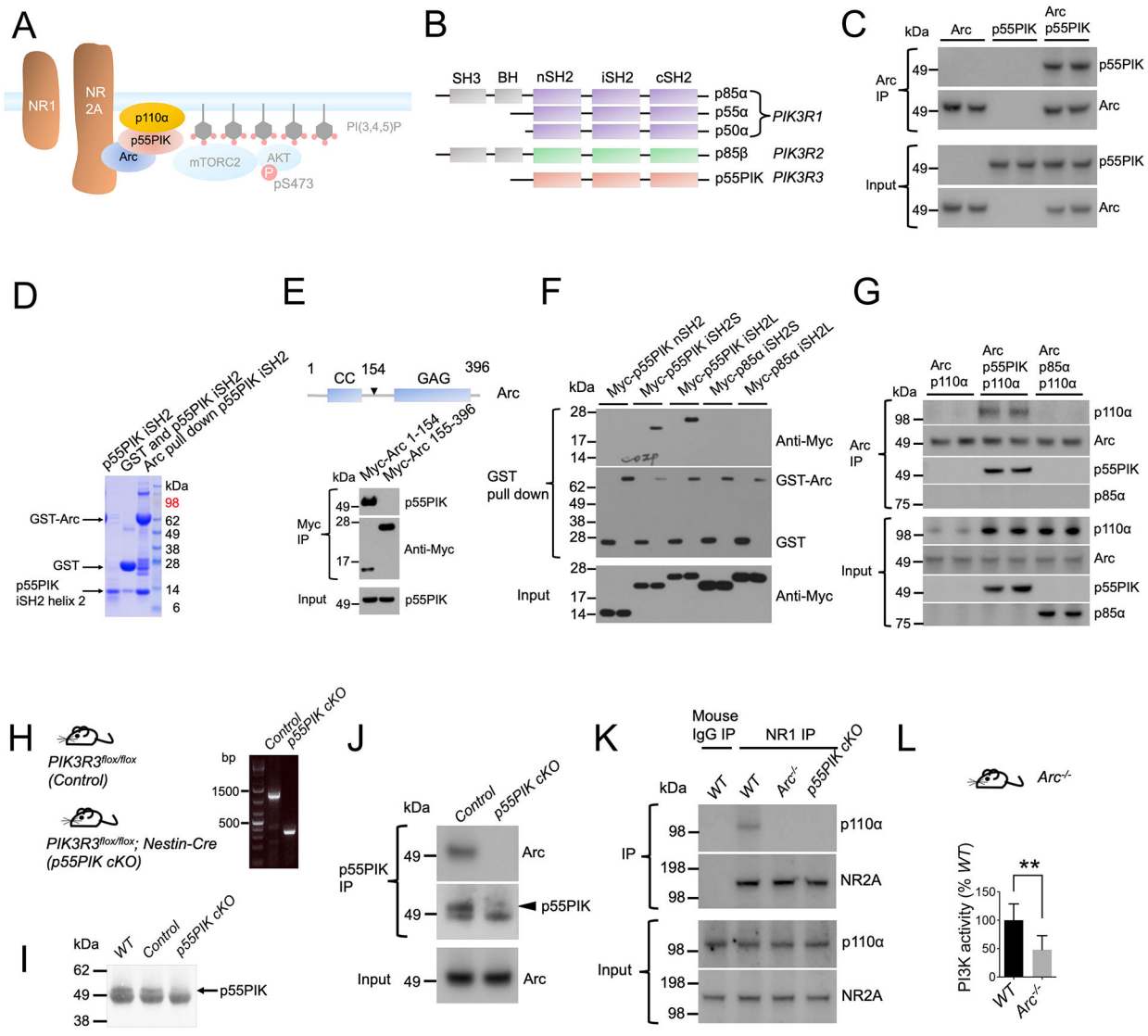

Figure 1. Arc couples NMDAR to p55PIK-PI3K.

(A) Diagram of NMDAR-Arc-p55PIK-PI3K-AKT signaling pathway highlighting the binding of Arc and p55PIK-PI3K to NMDAR. (B) PI3K regulatory subunit gene family and domain organization. SH3: Src Homology 3 domain. BH: Bcl-2 Homology domain. SH2: Src Homology 2 domain (n: NH2 terminal, i: Inter, c: COOH terminal). (C-D) Arc binds p55PIK. (C) Immunoblotting of p55PIK co-IP with Arc (anti-Arc antibody for IP and anti-p55PIK antibody for immunoblotting) from HEK 293T cells. (D) Coomassie blue stain of recombinant p55PIK iSH2 helix 2 pulled down together with recombinant GST-Arc. (E) Arc N-terminus that includes coiled-coil domain (CC) mediates Arc-p55PIK binding in HEK 293T cells. (F) Arc selectively binds p55PIK iSH2 domain; Short (helix 1 and helix 2) or Long (entire iSH2 domain) in HEK 293T cells. (G) p110α forms tri-molecular complex with Arc-p55PIK but not Arc-p85α in HEK 293T cells. p110α expression is stabilized by both p85α and p55PIK. (H) Genomic PCR showing excision of p55PIK exon 4 in *p55PIK cKO* mouse forebrain. (I) Immunoblotting showing depletion of p55PIK protein in *p55PIK cKO* mouse forebrain (upper band). p55PIK was enriched by IP before immunoblotting. (J)

Arc co-IPs with p55PIK in mouse forebrain lysate. (K) p110α co-IPs with NMDAR in *WT* but not in *Arc*$^{-/-}$ or *p55PIK cKO* mouse forebrain lysate. (L) PI3K activity is reduced in *Arc*$^{-/-}$ mouse forebrain measured by the conversion rate of PI(4,5)P to PI(3,4,5)P (n=6). n represents numbers of mice used in each group. Error bar indicates standard deviation (SD). Quantitative data were analyzed using two-tailed Student's t-test. ** P<0.01.

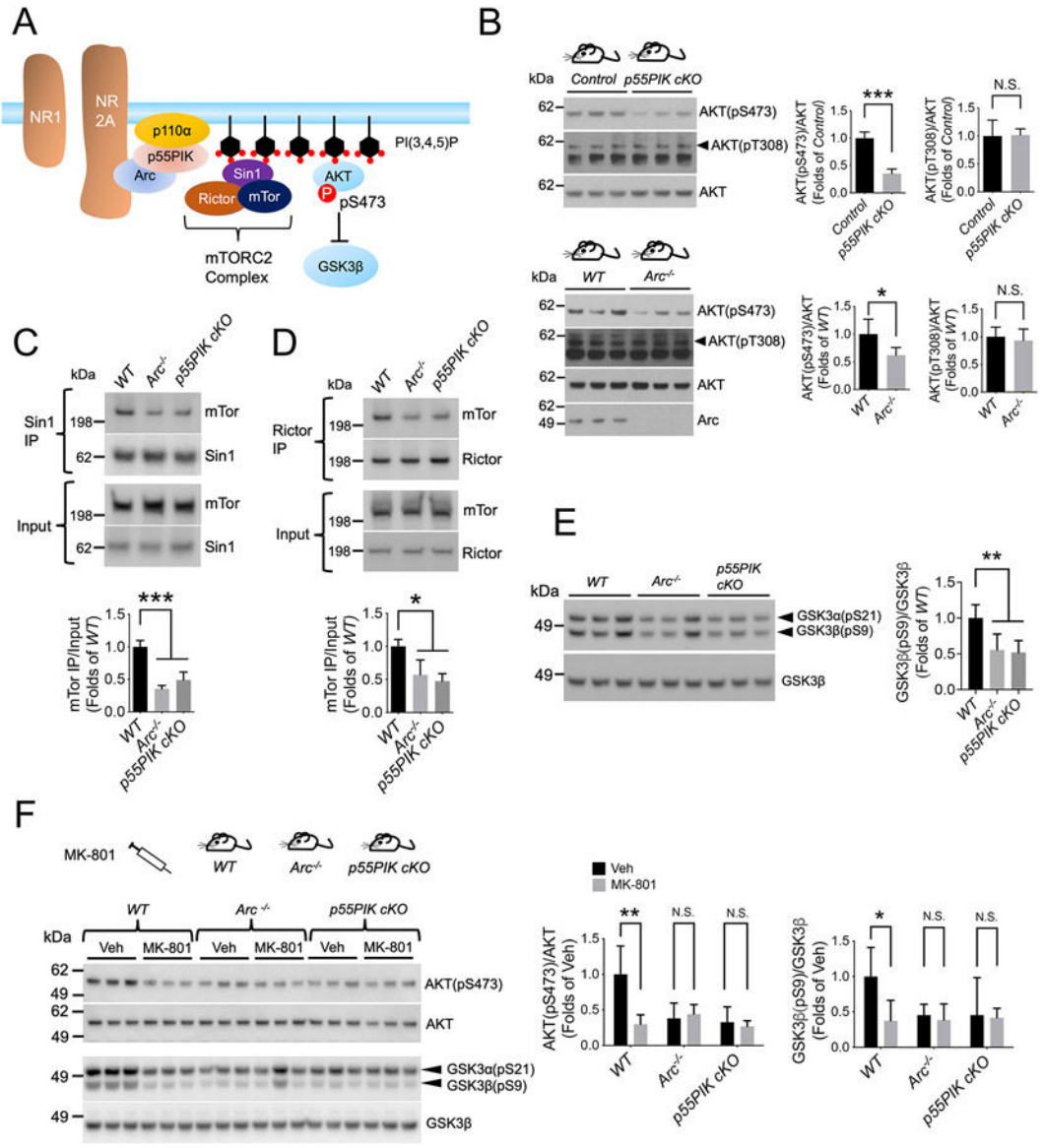

Figure 2. Arc and p55PIK mediate NMDAR-AKT activation in brain.

(A) Diagram of NMDAR-Arc-p55PIK-PI3K-AKT signaling pathway. (B) AKT(pS473) phosphorylation is reduced in the forebrain of *p55PIK cKO* (n=6) and $Arc^{-/-}$ mice (n=6) while AKT(pT308) keeps the same. (C-D) mTORC2 complex integrity assayed by Sin1 (C) or Rictor (D) co-IP of mTor is reduced in $Arc^{-/-}$ (n=4) and *p55PIK cKO* mice (n=4) forebrain lysate. (E) GSK3β(pS9) is reduced in $Arc^{-/-}$ (n=6) and *p55PIK cKO* (n=6) mice forebrain. (F) MK-801 (1 mg/kg s.q.; 1 hr) reduces AKT(pS473) and GSK3β(pS9) in *WT* but not $Arc^{-/-}$ or *p55PIK cKO* mouse forebrain (n=6). n represents numbers of mice used in each group. Error bar indicates standard deviation (SD). Quantitative data were analyzed using two-tailed Student's t-test. * P<0.05, ** P<0.01, *** P<0.001, N.S. no significant difference.

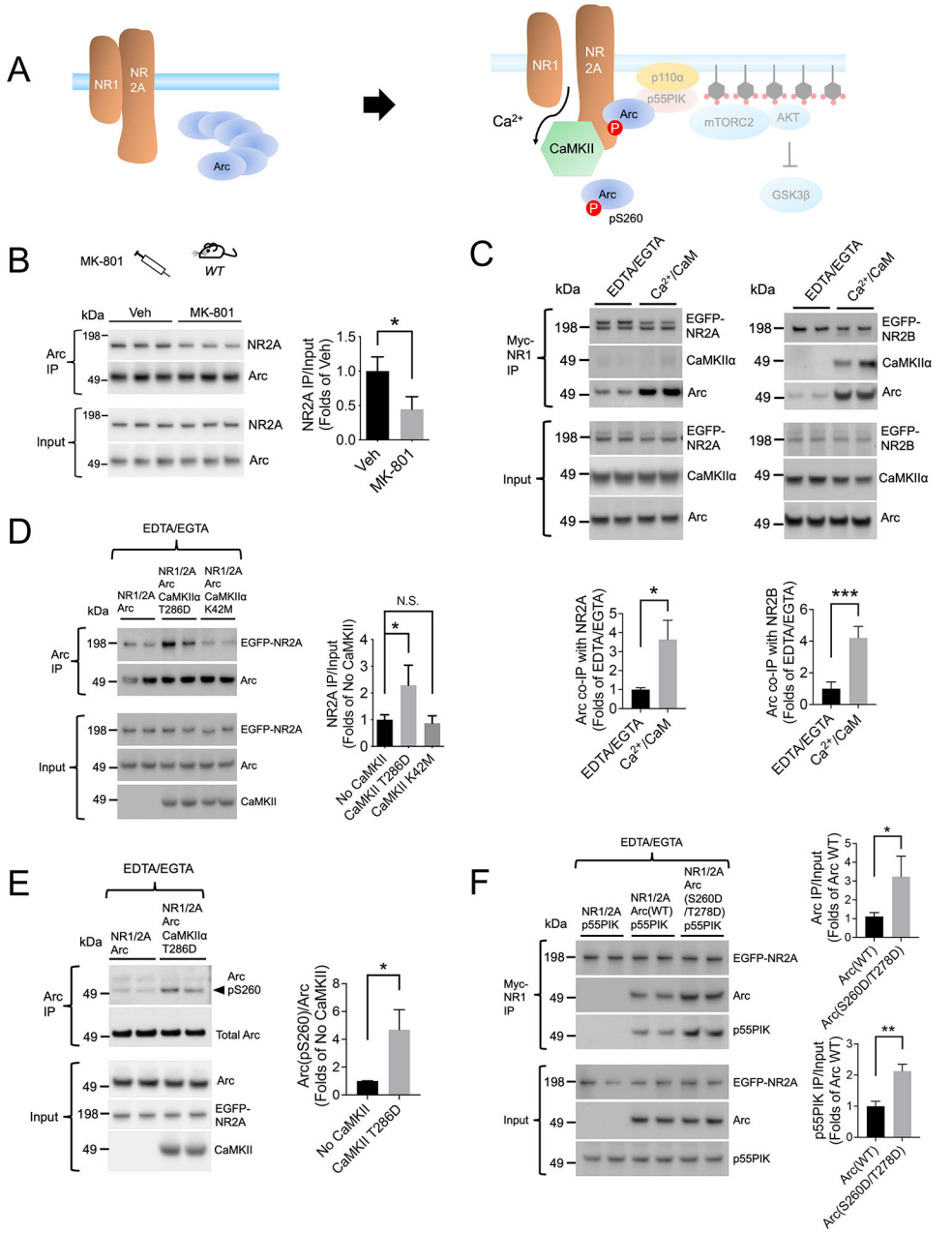

Figure 3. CaMKII activity enhances NMDAR-Arc-PI3K complex assembly.

(A) Diagram of NMDAR-Arc-p55PIK-PI3K-AKT signaling pathway showing phosphorylation of Arc prevents its oligomerization and enhances NMDAR binding. (B) MK-801 (1 mg/kg s.q.; 1 hr) reduces NR2A co-IP with Arc (n=6) in *WT* mouse forebrain lysate. (C) Ca^{2+} and calmodulin (CaM) increase Arc and CaMKIIα co-IP with NMDAR in HEK 293T cell lysate. NMDAR (Myc-NR1 and EGFP-NR2A or -NR2B), CaMKIIα and Arc were transgenically expressed in HEK 293T cells. EDTA/EGTA(5 mM) or Ca^{2+}(1 mM)/CaM(3 mM) were added to cell lysate during IP. (D) NMDAR-Arc binding in HEK 293T cells is increased by co-expression of active CaMKIIα (T286D) but not kinase-dead CaMKIIα (K42M) in the presence of EDTA/EGTA. (E) CaMKIIα (T286D) phosphorylates

Arc(S260) in HEK 293T cells. Arc(pS260) was blotted with phospho-specific antibody after IP. (F) Arc phosphomimic mutations (S260D and T278D) increase NMDAR-Arc-p55PIK complex formation in HEK 293T cells. Quantification was done with 4 transfection replicates in (C-F). n in (B) represents number of mice in each group. Error bar indicates SD. Quantitative data were analyzed using two-tailed Student's t-test. * $P<0.05$, ** $P<0.01$, *** $P<0.001$, N.S. No significant difference.

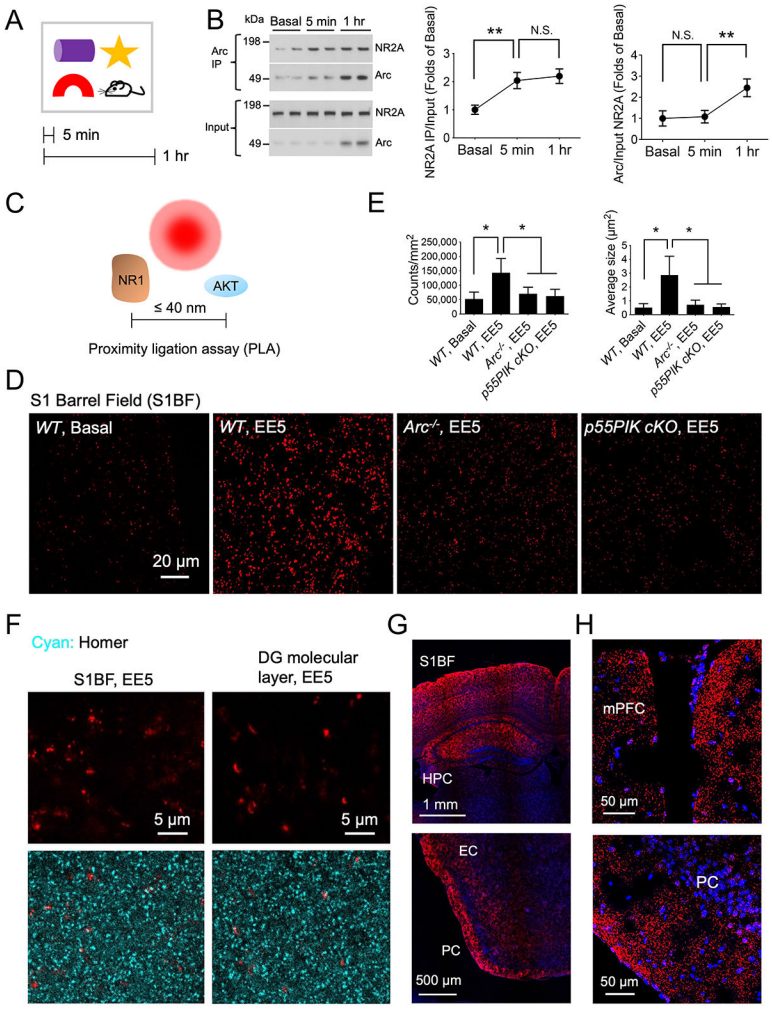

Figure 4. Novel environment induces rapid NMDAR-Arc complex formation and AKT recruitment to NMDAR proximal membrane.

(A) Diagram of enriched environment (EE). Mice were sacrificed from home cage (Basal) or after 5 min or 1 hr in EE. (B) Rapid increase of NR2A co-IP with Arc from cortical lysates that precedes significant increase of Arc (n=4 at each time point). (C-E) EE for 5 min (EE5) increased NMDAR-AKT physical proximity (PLA; red) in S1 Barrel Field (S1BF) of *WT* but not $Arc^{-/-}$ or *p55PIK cKO* mice. Quantification was done with brain slices from 4 mice each group. (F) EE5-induced NMDAR-AKT PLA localizes to sparse synapses labelled with Homer staining in S1BF and dentate gyrus (DG). (G-H) EE5-induced NR1-AKT PLA in different brain regions. (G) Images taken using 5X objective. Up: Sensory cortex (S1BF) and hippocampus (HPC); Bottom: Entorhinal cortex (EC) and piriform cortex (PC). (H) Images taken using 25X objective. Up: Medial prefrontal cortex (mPFC); Bottom: Piriform cortex (PC). Blue: DAPI stain. Error bar indicates SD. Data were analyzed using two-tailed Student's t-test. * P<0.05, ** P<0.01, N.S. no significant difference.

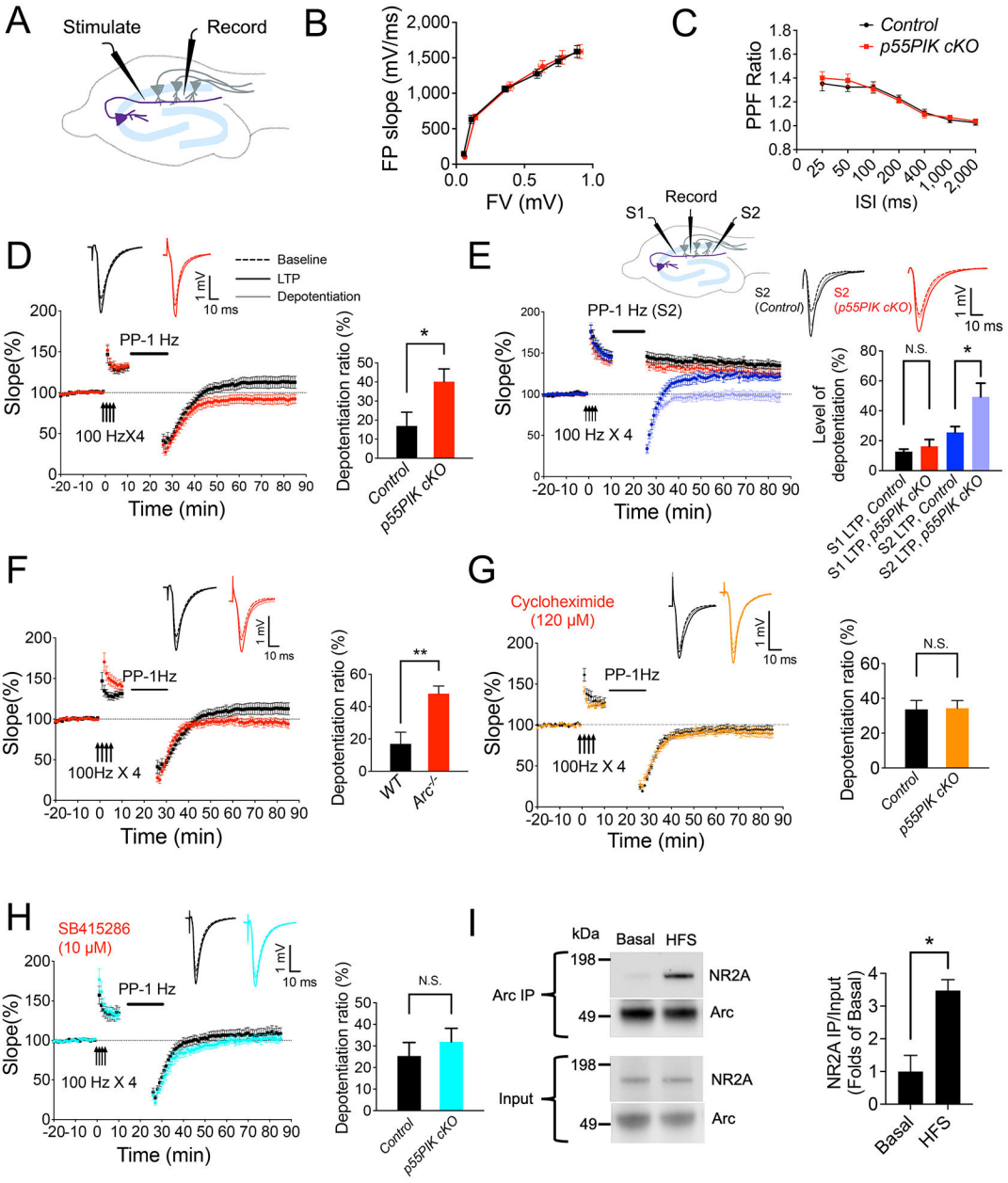

Figure 5. NMDAR-Arc-p55PIK-PI3K-AKT mediates LTP inhibition of depotentiation by suppressing GSK3ß.

(A) Diagram of Schaffer-CA1 hippocampal slice recordings comparing *control* (*PIK3R3*$^{flox/flox}$) and *p55PIK cKO* (*PIK3R3*$^{flox/flox}$*; Nestin-Cre*). (B-C) Baseline synaptic transmission. (B) Field potential (FP) slope relative to fiber volley (FV) (n=10). (C) Paired-pulse facilitation (PPF) ratio (n=8), ISI: Interstimulus interval. (D) Depotentiation to PP-1 Hz following LTP is increased in *p55PIK cKO* (n=13). Right: Percent of depotentiation comparing LTP levels from 81 to 85 min to LTP levels from 6 to 10 min (same as in E, F,G and H). (E) Depotentiation of *p55PIK cKO* LTP is specific to input synapses (n=9). PP-1 Hz applied to different input had no effect on newly induced LTP. (F) Depotentiation to PP-1 Hz following LTP is also increased in *Arc*$^{-/-}$ (n=14). (G) LTP

resistance to depotentiation requires new protein synthesis (n=10). Cycloheximide (120 μM) was added 30 min before recording. (H) Pretreatment with GSK3β (SB415286, 10 μM, added during recover incubation 1 hr before LTP induction) prevented the difference in depotentiation observed between untreated *control* and *p55PIK cKO* slices (n=11). (I) LTP induced NMDAR-Arc complex formation 10 min after tetanic stimulus in mouse hippocampal slices. Four hippocampal slices from each mouse were pooled together for enough material. Quantification was done with 3 individual mice. HFS: High frequency stimulus. n represents numbers of hippocampal slices prepared from at least 3 mice per genotype. Error bar indicates standard error of the mean (SEM). * $P<0.05$, ** $P<0.01$, N.S. no significant difference in two-tailed Student's t-test.

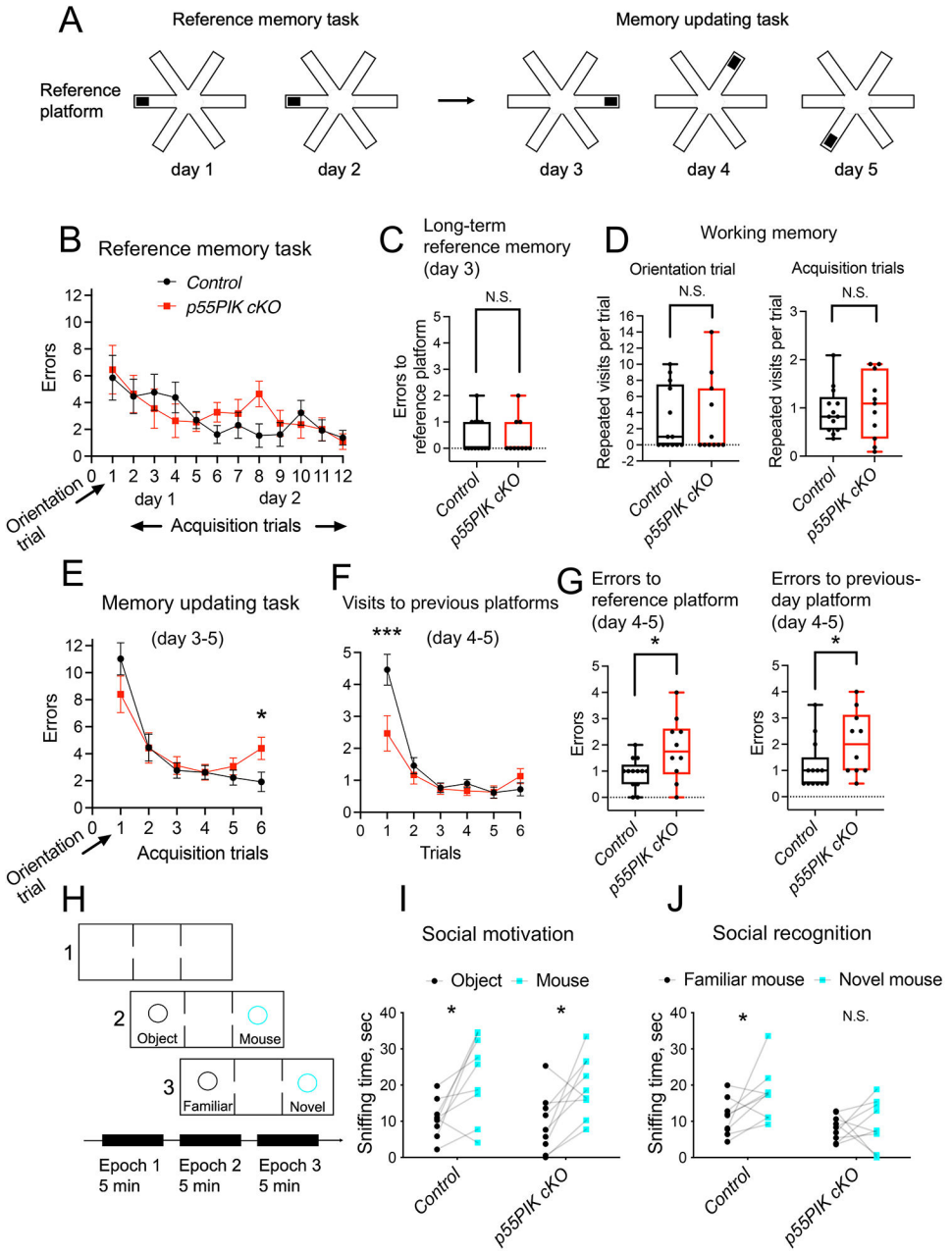

Figure 6. *p55PIK cKO* mice exhibit deficits in memory updating.

(A) Scheme of behavioral protocol used in the Radial Water Maze (RWM). Each day of training mice had 6 trials in which they were required to find a hidden platform. The location of the platform (filled rectangle) was kept the same in days 1-2 (reference memory task) and changed daily in days 3-5 (memory updating task). (B-D) Performance of *p55PIK cKO* mice (n=11) was similar to *control* mice (n=13) in days 1-2. (B) Number of errors to find the 1st location of the hidden platform ('reference platform') in days 1-2 of the training. (C) Number of errors to find the reference platform after a 20 hr delay assessed during the orientation trial on day 3 of the training. (D) Repeated visits to the same arms during orientation and acquisition trials in days 1-2. (E-G) Performance of *p55PIK cKO* mice was

impaired in days 3-5. The same mice were used as in (B-D). (E) Number of errors to find a daily new platform location averaged across days 3-5. *p55PIK cKO* mice made more errors than *control* mice in the last trial. (F) Visits to the previous day's platform location averaged across days 4-5. *p55PIK cKO* mice made less previous platform visits than *control* mice in the orientation trials. (G) Number of errors in orientation trials averaged across days 4-5. Number of errors to the 1st visit of the reference platform location (from training days 1-2; Left) or the previous day's platform location (Right). (H) Scheme of a three-chamber social interaction test. (I) Sniffing times for social (mouse) and non-social objects in Epoch 1 of testing for social motivation. No differences in social preferences were detected between *p55PIK cKO* (n=9) and *control* (n=9) mice. (J) Sniffing times for familiar and novel mouse assessed during testing for social recognition (Epoch 2). In contrast to *control, p55PIK cKO* mice demonstrated no preference for novel mouse. n represents numbers of mice in each group. Error bar indicates SEM in (B), (E), (F). In (C-D) and (G) boxes indicate an inter-quartile range and error bars indicate a min to max range. * $P<0.05$, *** $P<0.001$, N.S. no significant difference in ANOVA post-hoc tests or Kruskal-Wallis ANOVA.

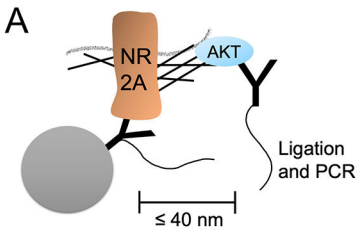

B

	Disease stage	BRAAK	Brain region
Cohort #1	Late	4-6	MTG
Cohort #2	Early	2-3	OFC

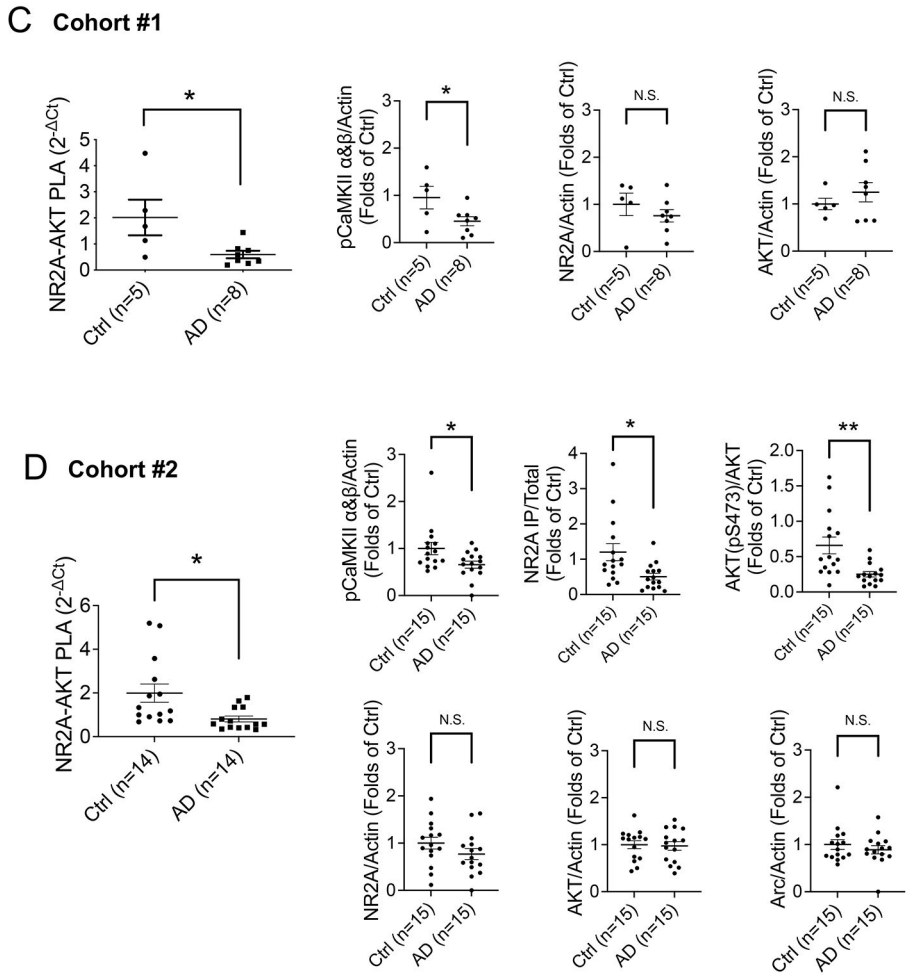

Figure 7. NMDAR-AKT complex formation is reduced in Alzheimer's disease brain.

(A) Diagram of homogenate-based proximity ligation assay. Proteins closely associated (≤ 40 nm) in detergent-free brain homogenate will be detected using oligonucleotide-conjugated antibody, connector ligation, and quantitative PCR. (B) Summary of clinical information of two cohorts of human brain samples. BRAAK: neurofibrillary tangle (NFT) stage. MTG: middle temporal gyrus. OFC: orbitofrontal cortex. (C-D) Quantitative PLA analysis and immunoblotting of NMDAR-AKT signaling cascade in cohort 1 (C) and cohort 2 (D) brain samples. ΔCt is Ct (threshold cycle) number subtracted by average Ct in AD group. All immunoblotting images are presented in Supplemental Figure 6. n represents

sample number. Error bar indicates SEM. P value was calculated using unpaired two-tailed Student's t-test. * P<0.05, ** P<0.01, N.S. no significant difference.

KEY RESOURCES TABLE

Resource Type	Specific Reagent or Resource	Source or Reference	Identifiers	Additional Information
Add additional rows as needed for each resource type	Include species and sex when applicable.	Include name of manufacturer, company, repository, individual, or research lab. Include PMID or DOI for references; use “this paper” if new.	Include catalog numbers, stock numbers, database IDs or accession numbers, and/or RRIDs. RRIDs are highly encouraged; search for RRIDs at https://scicrunch.org/resources.	Include any additional information or notes if necessary.
Antibody	Mouse monoclonal anti-Arc	Doi:10.1016/j.neuron.2015.03.030	N/A	
	Rabbit polyclonal anti-Arc	Doi:10.1016/j.neuron.2015.03.030	N/A	
	Rabbit polyclonal anti-Arc(pS260)	Doi:10.1016/j.molcel.2019.05.004	N/A	
	Rabbit polyclonal anti-p55PIK	This paper	N/A	
	Goat polyclonal anti-p55PIK	Santa Cruz	Cat# sc-48644, RRID:AB_2163477	
	Rabbit polyclonal anti-p85α	Cell Signaling	Cat# 4292, RRID:AB_329869	
	Rabbit monoclonal anti-p110α	Cell Signaling	Cat# 4249, RRID:AB_2165248	
	Rabbit monoclonal anti-AKT(pS473)	Cell Signaling	Cat# 4060, RRID:AB_2315049	
	Rabbit monoclonal anti-AKT(pT308)	Cell Signaling	Cat# 4056, RRID:AB_331163	
	Rabbit monoclonal anti-GSK3α/β(pS21/pS9)	Cell Signaling	Cat# 8566, RRID:AB_10860069	
	Rabbit monoclonal anti-GSK3β	Cell Signaling	Cat# 9315, RRID:AB_490890	
	Rabbit polyclonal anti-NR2A	Millipore	Cat# 07-632, RRID:AB_310837	
	Rabbit polyclonal anti-NR2B	Cell Signaling	Cat# 4207, RRID:AB_1264223	
	Rabbit polyclonal anti-CaMKIIα	Cell Signaling	Cat# 3357, RRID:AB_2070308	
	Rabbit polyclonal anti-CaMKIIβ	Abcam	Cat# ab34703, RRID:AB_2275072	

Resource Type	Specific Reagent or Resource	Source or Reference	Identifiers	Additional Information
	Rabbit polyclonal anti-CaMKIIα/β(pT286/pT287)	Abcam	Cat# ab32678, RRID:AB_725893	
	Rabbit polyclonal anti-β-Actin	Abcam	Cat# ab8227, RRID:AB_2305186	
	Goat polyclonal anti-NR1	Sigma-Aldrich	Cat# SAB2500698, RRID:AB_10605816	
	Rabbit polyclonal anti-AKT	Cell Signaling	Cat# 9272, RRID:AB_329827	
	Mouse monoclonal anti-Homer	Santa Cruz	Cat# sc-17842, RRID:AB_627742	
	Mouse monoclonal anti-Sin1	Millipore	Cat# 05-1044, RRID:AB_1587253	
	Rabbit monoclonal anti-Sin1	Cell Signaling	Cat# 12860, RRID:AB_2798048	
	Rabbit monoclonal anti-Rictor	Cell Signaling	Cat# 9476, RRID:AB_10612959	
	Rabbit polyclonal anti-mTor	Cell Signaling	Cat# 2972, RRID:AB_330978	
	Mouse monoclonal anti-c-Myc	Santa Cruz	Cat# sc-40 AC, RRID:AB_2857941	
	Rabbit monoclonal anti-Myc-Tag	Cell Signaling	Cat# 2278, RRID:AB_490778	
	Mouse monoclonal anti-GST	Santa Cruz	Cat# sc-138, RRID:AB_627677	
Bacterial or Viral Strain	*E. coli* BL21 (DE3)	NEB	Cat# C2527	
	E. coli NEB Stable	NEB	Cat# C3040	
	E. coli DH5α	Doi:10.1016/j.neuron.2015.03.030	N/A	
Biological Sample	Human brain tissue	Johns Hopkins Medical Institute Brain Resource Center	N/A	
Cell Line	Human: HEK 293T	ATCC	CRL-3216	
Chemical Compound or Drug	(+)-MK 801 maleate	Tocris	Cat# 0924	
	(RS)-3,5-DHPG	Tocris	Cat# 0342	

Resource Type	Specific Reagent or Resource	Source or Reference	Identifiers	Additional Information
	SB 415286, GSK3 inhibitor	Tocris	Cat# 1617	
	Insulin (human) recombinant expressed in yeast	Tocris	Cat# 3435	
Commercial Assay Or Kit	PI3-Kinase Activity ELISA: Pico	Echelon Biosciences	K-1000S	
	Duolink Proximity Ligation Assay (Fluorescence)	Millipore Sigma	https://www.sigmaaldrich.com/US/en/technical-documents/protocol/protein-biology/protein-and-nucleic-acid-interactions/duolink-fluorescence-user-manual	
Deposited Data; Public Database				
Genetic Reagent	*PIK3R3* exon 4 genomic PCR forward primer: 5'-ACAACCATACCCATCCCAGA-3'	This paper	N/A	
	PIK3R3 exon 4 genomic PCR reverse primer: 5'-CAGCTCCACACAATGTAACGTC-3'	This paper	N/A	
	Arc^{P217F} knock-in mouse CRISPR sgRNA sequence: *5'-ACAGATCTTCGAGGACCCAC-3'*	This paper	N/A	
	Oligo plus conjugated to NR2A antibody (5AmMC6): 5'-CGCATCGCCCTTGGACTACGACTGACGAACCGCTTTGCCTGACTGATCGCTAAATCGTG-3'	This paper	N/A	
	Oligo minus conjugated to AKT antibody (3AmMO): 5'-TCGTGTCTAAAGTCCGTTACCTTGATTCCCCTAACCCTCTTGAAAAATTCGGCATCGGTGA-3'	This paper	N/A	
	Connector for NR2A-AKT PLA: 5'-TACTTAGACACGACACGATTTAGTTT-3'	This paper	N/A	
	Forward PLA primer: 5'-CATCGCCCTTGGACTACGA-3'	This paper	N/A	
	Reverse PLA primer: 5'-GGGAATCAAGGTAACGGACTTTAG-3'	This paper	N/A	
Organism/ Strain	Mouse, C57BL/6J	The Jackson Laboratory	RRID:IMSR_JAX:000664	
	Mouse: C57BL/6J, *Arc*$^{-/-}$	Doi:10.1016/j.cell.2011.09.036	N/A	
	Mouse: C57BL/6J, *Arc*$^{P217F/P217F}$ knock-in	This paper	N/A	
	Mouse: C57BL/6J, *PIK3R3*$^{flox/flox}$*; Nestin-Cre*	This paper	N/A	
Peptide, Recombinant Protein				
Recombinant DNA	pRK5 vector	Addgene	N/A	

Resource Type	Specific Reagent or Resource	Source or Reference	Identifiers	Additional Information
	pGEX-6P-1 vector	GE Healthcare	Cat# 28954648	
	pEBG vector	Addgene	Cat# 22227	
	pcDNA3.1-myc-NR1	Doi:10.1016/j.neuron.2004.09.029	N/A	
	pRK5-NR2A, pRK5-NR2B	Doi:10.1016/j.neuron.2004.09.029	N/A	
	pEGFP-NR2A, pEGFP-NR2B	Addgene	Cat# 17924, 17925	
	pRK5-CaMKIIα T286D, pRK5-CaMKIIα K42M	Richard Huganir Lab	N/A	
Sequence-Based Reagent				
Software; Algorithm	CCTop, CRISPR/Cas9 target online predictor	European Research Council	https://cctop.cos.uni-heidelberg.de:8043/	
	Image Lab	Bio-Rad	https://www.bio-rad.com/en-us/product/image-lab-software?ID=KRE6P5E8Z	
	ImageJ	NIH	https://imagej.nih.gov/ij/download.html	
	Zeiss Zen	Zeiss	https://www.zeiss.com/microscopy/us/products/microscope-software/zen.html	
	Igor Pro	WaveMetrics	https://www.wavemetrics.com/	
	ANY-maze	Stoelting	https://stoeltingco.com/Neuroscience/ANY-maze	
	TopScan	CleverSys	http://cleversysinc.com/CleverSysInc/csi_products/topscan-suite/#csi-software	
	GraphPad Prism 9	GraphPad	https://www.graphpad.com/scientific-software/prism/	
	Statistica 13.3	TIBCO	https://docs.tibco.com/products/tibco-statistica-13-3-0	
Transfected Construct	See Recombinant DNA			
Other				